Gastro Hep Advances 2022;1:253–264

ORIGINAL RESEARCH—BASIC

The G Protein-Coupled Receptor, VPAC1, Mediates Vasoactive Intestinal Peptide-Dependent Functional Homeostasis of the Gut Microbiota

Aaron C. Ericsson,[1] Manpreet Bains,[2] Zachary McAdams,[1] Justin Daniels,[2] Susheel B. Busi,[3] James A. Waschek,[4] and Glenn P. Dorsam[2]

[1]Department of Veterinary Pathobiology, University of Missouri Metagenomics Center, College of Veterinary Medicine, University of Missouri, Columbia, Missouri; [2]Department of Microbiological Sciences, College of Agriculture, Food Systems and Natural Resources, North Dakota State University, Fargo, North Dakota; [3]Department of Systems Ecology, Luxembourg Centre for Systems Biomedicine, University of Luxembourg, Esch-sur-Alzette, Luxembourg, and [4]Department of Psychiatry and Biobehavioral Sciences, Intellectual and Developmental Disabilities Research Center, Semel Institute for Neuroscience and Human Behavior/Neuropsychiatric Institute, University of California, Los Angeles, Los Angeles, California

BACKGROUND AND AIMS: Vasoactive intestinal peptide (VIP) is a neuropeptide involved in the regulation of feeding behavior and circadian rhythms, metabolism, and immunity. Previous studies revealed the homeostatic effects of VIP signaling on the gut microbiota. VIP-deficient mice demonstrate a gut microbiota dysbiosis characterized by reduced α-diversity and decreased relative abundance (RA) of Gram-positive *Firmicutes*. However, the mechanism by which VIP signaling affects changes in the microbiota is unknown. **METHODS:** To investigate the role of the 2 cognate G protein-coupled receptors for VIP (VPAC1 and VPAC2) in VIP-mediated homeostasis of the microbiota, fecal samples from VPAC1- and VPAC2-deficient, heterozygous, and wild-type littermate mice were assessed via targeted amplicon sequencing. Their microbiota profiles were additionally compared with microbiota from VIP-deficient, heterozygous, and wild-type littermates, where genotype-dependent changes in the composition and predicted function of each cohort were compared. **RESULTS:** While wild-type mice in each line differed in α-diversity and β-diversity, consistent changes in both metrics were observed in VIP-deficient and VPAC1-deficient mice. This includes a dramatic reduction in α-diversity, increased RA of *Proteobacteria* and *Bacteroidetes*, and decreased RA of *Lachnospiraceae*, *Ruminococcaceae*, *Muribaculaceae*, and *Rikenellaceae*. Specific amplicon sequence variants and predicted functions found to differ significantly based on VIP or VPAC1 genotype were concordant in their directions of change. Multiplatform predicted functional profiling suggested a defective VIP-VPAC1 axis was associated with reduced amino acid degradation along with reduced quinol and quinone biosynthesis. Furthermore, alterations in predicted functions include increased sugar degradation, nitrate reduction, and fatty acid biosynthetic pathways, among other changes. **CONCLUSION:** We conclude that VIP signaling through VPAC1 is critical for the maintenance of normal function of the gut microbiota.

Keywords: Neuropeptide; Microbiome; Gut Dysbiosis; *Firmicutes*; Microbiota

Introduction

Vasoactive intestinal peptide (VIP) is a 28-amino-acid neuropeptide with a broad expression profile regulating diurnal feeding behavior and taste perception,[1] metabolism,[2] and immunity.[3] VIP is delivered by the peripheral nervous system to numerous organs, including the mucosa-associated lymphoid tissues of the pulmonary and gastrointestinal tract (GIT).[4] VIP signals with high affinity (K_d = 1 nM) through at least 2 endogenous G protein-coupled receptors, called VIP/pituitary adenylyl cyclase-activating polypeptide (VPAC) 1 and VPAC2.[5,6] VIP signaling is responsible for numerous biological effects within the GIT, including digestive enzyme secretion,[7] ion homeostasis,[8,9] relaxation phase of peristalsis,[10,11] mucus secretion,[12] mucosal immunity,[13] and intestinal epithelial cell homeostasis (eg, Goblet cells) and barrier integrity.[14] Importantly, a link between VIP deficiency and reduced expression of a key transcriptional master regulator for intestinal barrier integrity and function, *caudal* related homeobox transcription factor 2 (CDX2), highlights the profound signaling influence of VIP on homeostasis within the GIT. Moreover, VIP-deficient mice have significant morphological abnormalities, including shorter crypt and intestinal lengths, and thickening of smooth muscle tissue surrounding the small intestines,[12,14] demonstrating the central role VIP plays in GIT function and homeostasis.

Abbreviations used in this paper: **ASV, amplicon sequence variant; CDX2, caudal type homeobox 2; GD, Graves' disease; GIT, gastrointestinal tract; HET, heterozygous; PBMC, Peripheral blood mononuclear cell; PERMANOVA, permutational multivariate analysis of variance; RA, relative abundance; VIP, Vasoactive intestinal peptide; VIPAC, VIP/pituitary adenylyl cyclase-activating polypeptide; WT, wild-type.**

Most current article

Copyright © 2022 The Authors. Published by Elsevier Inc. on behalf of the AGA Institute. This is an open access article under the CC BY-NC-ND license (http://creativecommons.org/licenses/by-nc-nd/4.0/).

2772-5723
https://doi.org/10.1016/j.gastha.2021.11.005

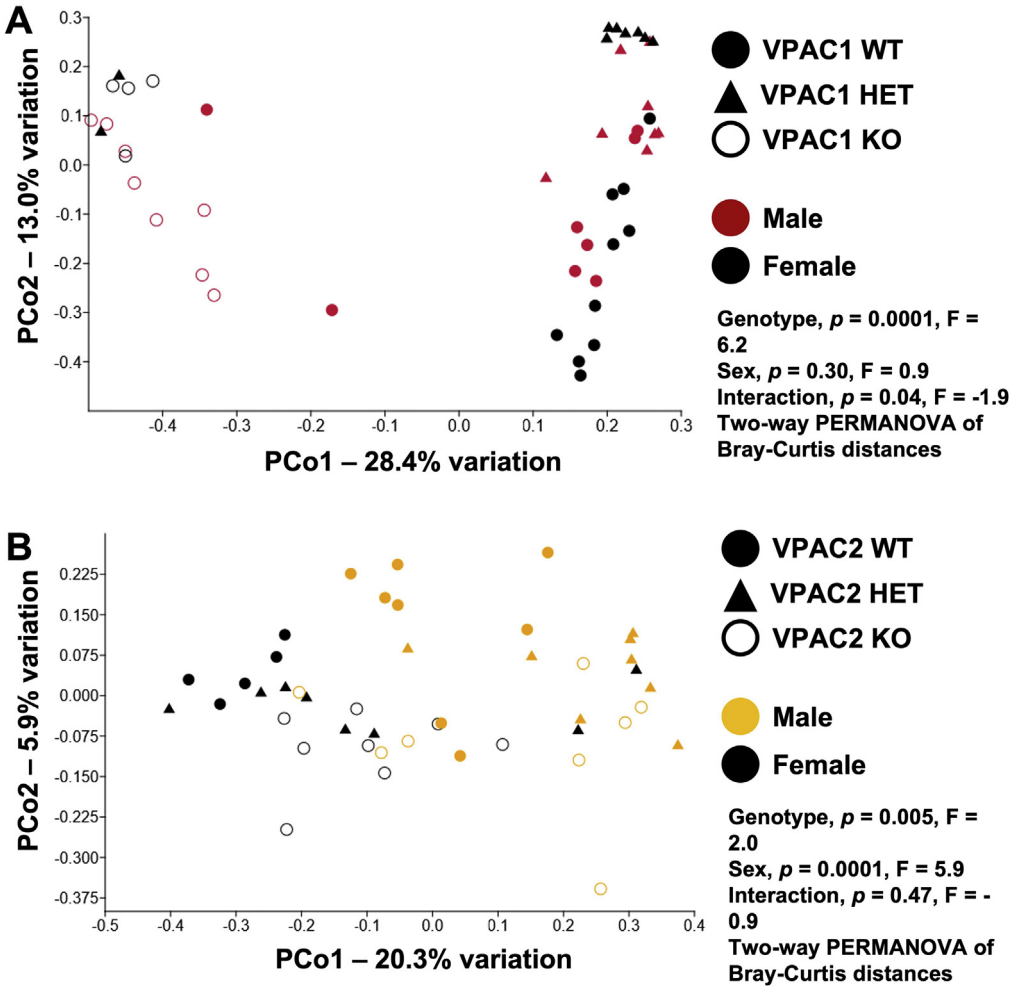

Figure 1. Genotype-dependent differences in fecal β-diversity are greater in VPAC1 line than in VPAC2 line. (A) Principal coordinate analysis (PCoA) plot showing genotype- and sex-dependent effects on Bray-Curtis similarities of fecal samples from male and female, VPAC1 WT, VPAC1 HET, and VPAC1 KO littermates (legend at right); results of two-way PERMANOVA with genotype and sex as fixed variables shown at lower right. (B) PCoA plot showing the same comparisons in fecal samples from male and female VPAC2 WT, VPAC2 HET, and VPAC2 KO littermates (legend at right); results of two-way PERMANOVA with genotype and sex as fixed variables shown at lower right.

It is now well-established that a stable GIT environment is important for homeostasis of the gut microbiota.[15] This "invisible metabolic organ" consists of trillions of microorganisms including bacteria, fungi, archaea, eukaryotic parasites, and viruses that play vital roles in host physiology, metabolism, and immunity (reviewed by Hooper and Gordon[16]). Dysbiosis, or compositional change in the gut microbiota associated with adverse health conditions or certain insults to the gut microbiota (eg, antibiotics), likely contributes to additional adverse sequelae including inflammation. Recently, our group reported that VIP-deficient mice are associated with an altered gut microbiota compared with wild-type (WT) littermates as assessed by 16S rRNA amplicon sequencing.[17] The identity of the specific VIP receptor driving these changes in the gut microbiota, however, remained unknown. Both VPAC1 and VPAC2 are expressed within the gut, albeit by different cell types.[18,19] To determine whether one or both of these receptors are involved in the previously observed homeostatic influence of VIP on the gut microbiota, mice deficient for VPAC1 or VPAC2 (VPAC1 KO and VPAC2 KO, respectively) were compared with WT and heterozygous (HET) littermates, as well as previous data from VIP KO, HET, and WT littermates. In addition, targeted amplicon data were analyzed using 2 separate platforms designed to predict functional capacity (PICRUSt2 and FAPROTAX), to identify consensus candidate microbial pathways affected by loss of VIP signaling in the host.

Results

Genotype-Dependent Phylogenetic Differences in VPAC1 and VPAC2 Deficient Mice

Sequencing of 16S rRNA amplicon libraries generated from a total of 48 mice from the VPAC1 line and 45 mice from the VPAC2 line resulted in a total of 3,616,234 and 3,593,086 high-quality sequence reads, respectively. Samples from the VPAC1 line were collected from VPAC1 WT ($n = 11$ female, 8 male), VPAC1 HET ($n = 9$ female, 8 male), and VPAC1 KO ($n = 4$ female, 8 male) littermate mice. Samples from the VPAC2 line included those from VPAC2 WT ($n = 5$ female, 8 male), VPAC2 HET ($n = 8$ female, 8 male), and VPAC1 KO ($n = 8$ female, 8 male) littermate mice.

VPAC1- and VPAC2-associated effects on the microbiota were visualized via principal coordinate analysis (PCoA) using Bray-Curtis similarities, and the significance and effect size of comparisons were determined using permutational multivariate analysis of variance (PERMANOVA). Within the VPAC1 line, there was a clear separation of VPAC1 KO samples from their WT and HET littermates along PCo1, with no

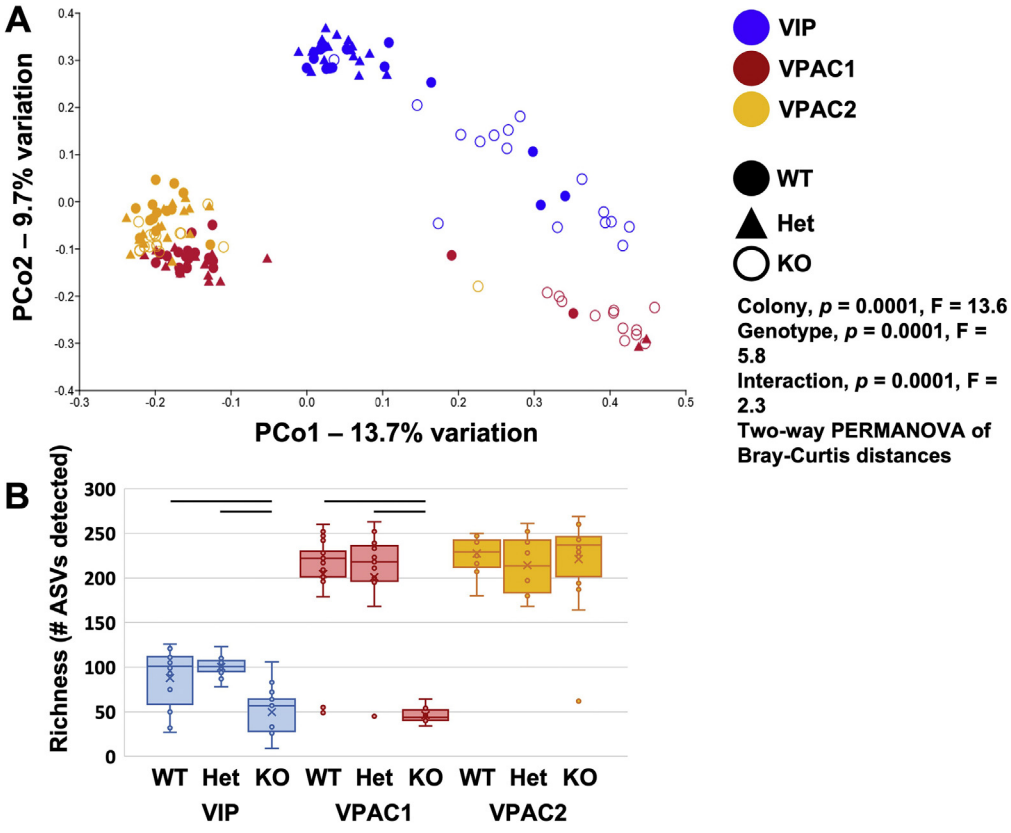

Figure 2. VPAC1-dependent changes in fecal β-diversity and α-diversity mirror VIP-dependent changes. (A) Principal coordinate analysis plot showing colony- and genotype-dependent effects on Bray-Curtis similarities of fecal samples from WT, HET, and KO littermates within the separate VIP, VPAC1, and VPAC2 lines (legend at right); results of two-way PERMANOVA with colony and genotype as fixed variables shown at lower right. (B) Tukey box plot of the detected richness in the same fecal samples; lines represent significant ($P < .05$, ANOVA on ranks) differences between groups in *post hoc* comparisons (Dunn's method), performed separately within each line.

apparent influence of sex. Results of a two-way PERMANOVA confirmed a significant genotype-dependent effect ($P = .0001$, $F = 6.2$) and a lack of sex-dependent effect ($P = .30$, $F = 0.9$) (Figure 1A). In contrast, similar comparisons within the VPAC2 line revealed reduced (albeit still significant) genotype-dependent differences in Bray-Curtis similarity ($P = .005$, $F = 2.0$) and an interesting sex-dependent difference ($P = .0001$, $F = 5.9$) (Figure 1B). Collectively, these data suggested that, while loss of either VPAC1 or VPAC2 was associated with differences in β-diversity, the effect was stronger in the context of VPAC1 deficiency.

VPAC1-Dependent Changes in Fecal β-Diversity and α-Diversity Mirror VIP-Dependent Changes

To compare the effects of VPAC1 and VPAC2 deficiency to each other, and to the effect of VIP deficiency, previously generated data from VIP WT ($n = 8$ female, 8 male), VIP HET ($n = 8$ female, 8 male), and VIP KO ($n = 8$ female, 7 male) littermates[17] were re-analyzed using an updated pipeline[20] alongside the data from this study. Visualization via PCoA revealed clear differences between the separate lines ($P = .001$, $F = 13.6$), with the VIP line being completely separated from the VPAC1 and VPAC2 lines (Figure 2A). Notably, the genotype-associated differences in β-diversity within the VIP and VPAC1 lines appeared to follow similar patterns, with samples from VIP KO and VPAC1 KO mice separating from their WT and HET littermates in a similar direction. Assessment of the third principal coordinate revealed substantial overlap of samples from VIP- and VPAC1-sufficient mice and samples from VIP KO and VPAC1 KO mice (Figure A1). In comparison to the differences between lines or the genotype-associated differences within the VIP and VPAC1 lines, the genotype-associated differences within the VPAC2 line were minor, based on F values. Comparisons of α-diversity within each line showed a similar pattern with clear differences between baseline α-diversity in different lines and similar genotype-associated reductions in the VIP and VPAC1 lines (Figure 2B). Analysis within each line detected significant differences between samples from VIP KO mice and their littermates ($P < .001$, ANOVA) and between samples from VPAC1 KO mice and their littermates ($P < .001$) and no effect of VPAC2 deficiency on richness ($P = .43$). A similar analysis of Simpson diversity found identical genotype-associated differences within the VIP and VPAC1 lines ($P < .001$ for both, ANOVA) and a trend toward VPAC2-dependent differences ($P = .06$) (Figure A2). Collectively, these analyses suggest that similar genotype-dependent differences are manifested within the lines, which is reflected by the microbiota richness, α- and β-diversity, when either functional VIP or VPAC1 expression is lost.

VPAC1-Dependent Changes in Taxonomic Composition of Fecal Microbiota Reflect VIP-Dependent Changes

To identify the VIP- and VPAC1-dependent changes in community composition taxonomically, serial t-tests were

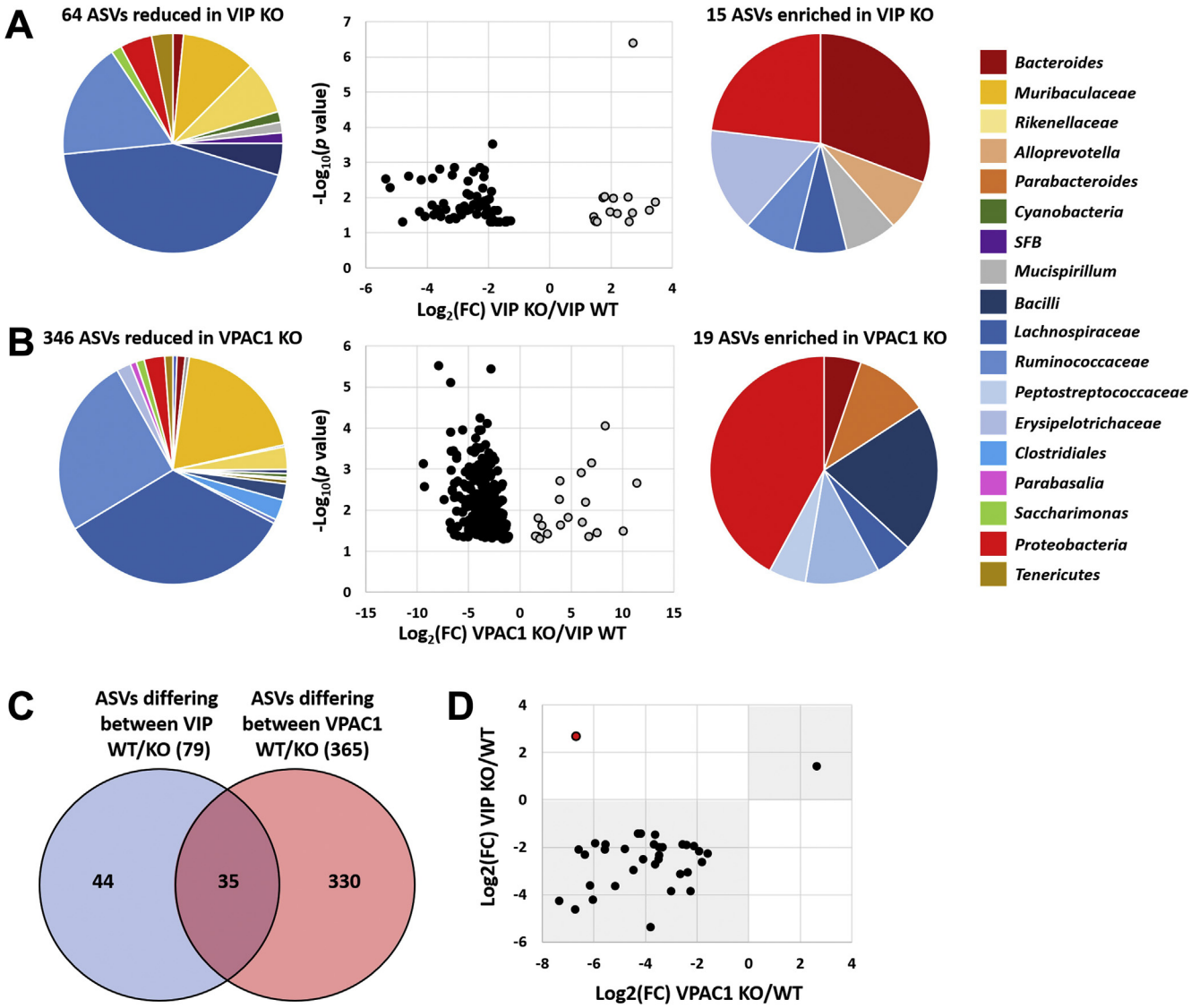

Figure 3. VPAC1-dependent changes in taxonomic composition of fecal microbiota reflect VIP-dependent changes. (A) Volcano plot showing the fold change (FC) of ASVs yielding a *P* value $< .05$ in serial t-tests of the relative abundance of all amplicon sequence variants (ASVs) in samples from VIP WT and VIP KO littermates, flanked by pie charts showing the taxonomic distribution of all ASVs found to be reduced (left) or enriched (right) in VIP KO mice relative to VIP WT littermates. (B) Volcano plot and pie charts arranged as (A), showing comparisons between VPAC1 WT and VPAC1 KO littermates. (C) Venn diagram showing the overlap in the 79 and 365 ASVs shown in the volcano plots, and (D) dot plot showing the agreement in direction of the genotype-dependent differences in the relative abundance of the 35 shared ASVs in each line; red dots indicate disagreement in the direction of change.

performed to test for differences between samples from WT and KO mice in the relative abundance (RA) of each amplicon sequence variant (ASV) individually. Those ASVs detected at a significantly increased or decreased RA in VIP WT mice relative to VIP KO, or in VPAC1 WT mice relative to VPAC1 KO mice, were compared (HETs were removed from these analyses to avoid imbalanced groups.). We opted to use raw, rather than false discovery rate-adjusted, *P* values as our goal was to compare genotype-associated effects on the microbiota, and trends in those effects were also of interest. Figure 3A shows a volcano plot of those ASVs yielding a raw *P* value $< .05$ and a Log_2(fold change) between VIP WT and VIP KO mice >2 or <-2, flanked by pie charts showing the taxonomic distribution, at the level of phylum, of ASVs detected at lower RA (left) or higher RA (right) in VIP KO mice compared with VIP WT mice (Table A1). A similar evaluation of all ASVs detected in the VPAC1 line revealed that, while the initial composition of the microbiota of these 2 lines differed, similar taxonomic differences were observed in the absence of VPAC1 (Figure 3B, Table A2). Specifically, the significantly reduced richness observed in both VIP KO and VPAC1 KO mice was reflected in the overall pattern of differences, with greater numbers of ASVs at a significantly reduced RA (as opposed

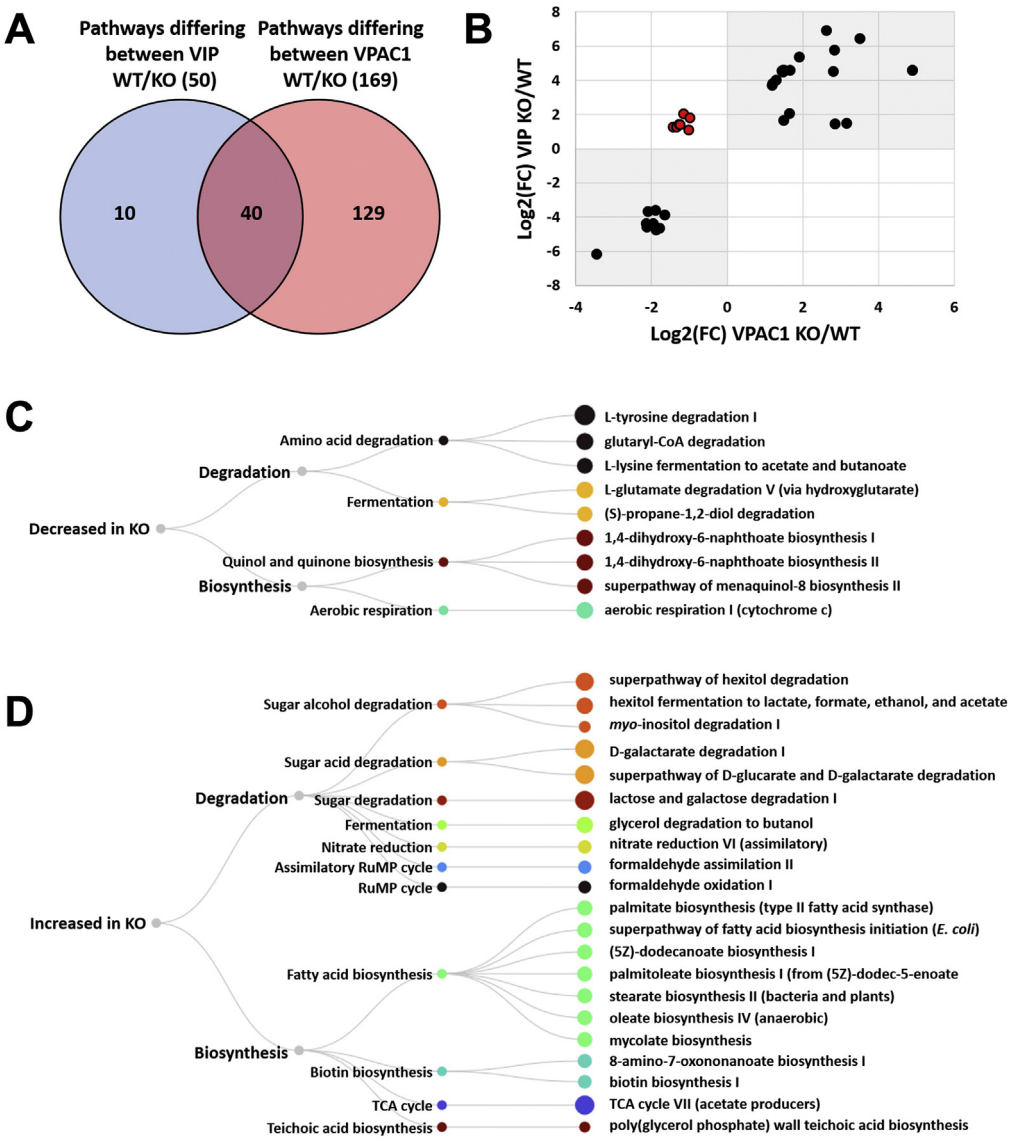

Figure 4. Similar functional changes are predicted in VIP KO and VPAC1 KO samples. (A) Venn diagram showing the overlap in the 50 functional pathways predicted to differ between samples from VIP KO and VIP WT mice and 169 functional pathways predicted to differ between samples from VPAC1 KO and VPAC1 WT mice, and (B) dot plot showing the agreement in the direction of the genotype-dependent differences in the predicted representation of the 40 shared functional pathways in each line, FC = fold change; red dots indicate disagreement in the direction of change. (C) Dendrogram showing the 9 predicted functional pathways detected at significantly lower levels in both VIP KO and VPAC1 KO samples, relative to those from WT littermates. Pathways, categorized according to superpathways (color), are shown at right, with node size representing mean FC between KO and WT littermates in both lines. (D) Dendrogram showing the twenty predicted functional pathways detected at significantly greater levels in both VIP KO and VPAC1 samples, relative to those from WT littermates.

to significantly increased RA) in the context of VIP or VPAC1 deficiency. Those ASVs with negative fold change values in KO mice included multiple taxa from the families *Lachnospiraceae*, *Ruminococcaceae*, *Muribaculaceae*, and *Rikenellaceae*, among others, while ASVs detected at greater RA in VIP KO and VPAC1 KO mice relative to their littermates included multiple *Proteobacteria*, *Bacteroidetes*, and related genera (eg, *Alloprevotella* and *Parabacteroides* spp.); several *Bacilli* within the VPAC1 line (*Lactobacillus* and *Streptococcus* spp.); and *Firmicutes* (eg, *Erysipelotrichaceae*, *Peptostreptococcaceae*), among others. A comparison of the 79 ASVs in the VIP contrast to the 365 ASVs in the VPAC1 contrast yielding raw P values $< .05$ found 35 shared ASVs (Figure 3C). Of those 35, 34 (97.1%) demonstrated the same direction of change (Figure 3D). Taken together, these data strongly suggest that signaling through VPAC1 is responsible for the previously reported homeostatic effects of VIP on the microbiota and that loss of a functional VIP-VPAC1 signaling axis results in a loss of Gram-positive *Firmicutes* complemented by an increased RA of predominantly Gram-negative taxa.

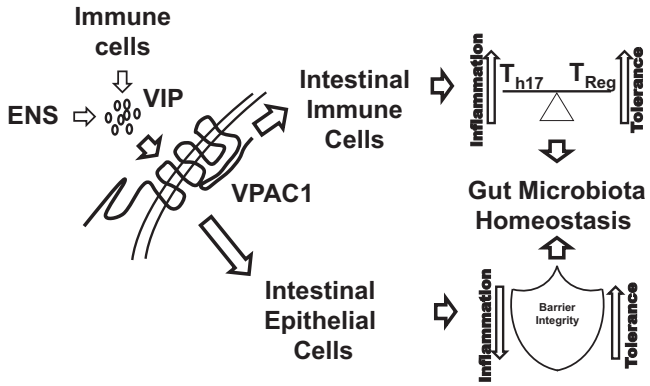

Figure 5. Hypothetical model for VIP→VPAC1 regulation of the gut microbiota. VIP ligand secreted by the enteric nervous system (ENS) and immune cells (T cells, B cells, and eosinophil cells) bind VPAC1 receptors on intestinal epithelial cells (e.g., Goblet cells) and immune cells (e.g., Tregs and mast cells,) that enhance intestinal barrier integrity and favor immune tolerance thereby regulating gut microbiota homeostasis.

Similar Functional Changes are Predicted in VIP KO and VPAC1 KO Samples

While these data suggest similar effects of VIP and VPAC1 deficiency on community composition, the microbiome is highly redundant, and the 2 lines of mice had distinct baseline compositions. With that in mind, our final goal was to identify and compare candidate microbial pathways predicted to have reduced or increased activity in the absence of VIP or VPAC1. Thus, to explore the effects of the observed compositional changes on predicted function of the microbiome, 2 different platforms (PICRUSt2[21] and FAPROTAX[22]) were used. As expected, there were several significant genotype-associated differences in the predicted microbial activity, as determined using PICRUSt2, within each line of mice. Of the 50 and 169 pathways found to differ significantly between VIP KO and VIP WT mice, or VPAC1 KO and VPAC1 WT mice, respectively, 40 were shared between the 2 lines (Figure 4A). As in the taxonomic comparisons, the direction of change in the shared functional pathways demonstrated high concordance (Figure 4B, Table A3). Functional pathways predicted to have reduced activity in the context of both VIP and VPAC1 deficiency included multiple amino acid degradation and quinol and quinone biosynthetic pathways, among others (Figure 4C). In contrast, pathways predicted to be increased in activity in both VIP- and VPAC1-deficient mice included an assortment of pathways associated with degradation of sugars (eg, lactose and galactose), sugar alcohols (eg, hexitols and myo-inositol), and sugar acids (eg, D-glucarate and D-galactarate); glycerol degradation; nitrate reduction; and the traditional and assimilatory ribulose monophosphate cycles (Figure 4D). Those changes were accompanied by increased activity of multiple biosynthetic pathways, including 7 separate pathways involved in fatty acid biosynthesis (eg, palmitate, stearate, and oleate), 2 pathways associated with biotin biosynthesis, and pathways related to the tricarboxylic acid cycle and teichoic acid biosynthesis.

We also assessed those pathways predicted to be significantly more or less active in only the VIP KO vs VIP WT contrast (10 pathways, Figure A3, Table A4) or in the VPAC1 KO vs VPAC1 WT contrast (128 pathways, Figure A4, Table A5). Additional genotype-dependent differences predicted in the VPAC1 line revealed consistencies and discrepancies with the shared pathways predicted to differ in both lines. For example, additional pathways related to biotin biosynthesis, sugar and sugar acid degradation, and the tricarboxylic acid cycle were predicted to be selectively increased in VPAC1 KO, all of which agree with the predicted functional differences shared by both VIP KO and VPAC1 KO mice. Similarly, the reduced tyrosine and lysine degradation predicted in both VIP KO and VPAC1 KO samples was complemented by a predicted increase in microbial production of both amino acids in the VPAC1 line. Examples of discrepant findings in the VPAC1 line include predicted increases in activity in numerous menaquinol biosynthesis pathways in the VPAC1 KO samples, in contrast to the predicted reduction in related pathways shared by both lines.

As a complement to the PICRUSt2-generated analyses, we also used the FAPROTAX platform to predict functional differences associated with the observed taxonomic changes. In general, informative genotype-dependent differences were more limited in both lines than the PICRUSt2 results. However, the few pathways predicted to be differentially present in VIP KO and VPAC1 KO lines generally agreed between each other, and with the PICRUSt2-predicted changes (Table A6). Specifically, nitrate reduction, predicted to be increased in activity in both VIP KO and VPAC1 KO mice compared with WT littermates using PICRUSt2, was also predicted to be increased in VPAC1 KO mice ($P = 3.6 \times 10^{-6}$) using FAPROTAX, with a similar trend ($P = .095$) in VIP KO mice. In contrast, nitrate reduction and nitrogen respiration were identified as being pathways at reduced levels in both VPAC1 KO and VIP KO mice.

Discussion

Our data collectively show that genetic deletion of VPAC1 in homozygous mutant (KO) mice was associated with reduced microbial diversity (α-diversity) and substantial changes in the gut microbiota composition (β-diversity) compared with HET or WT littermates, irrespective of sex. In contrast, VPAC2 deficiency did not differ in α-diversity but did show statistically significant β-diversity with a sex difference. However, these changes were subtle relative to the differences found in the VPAC1 colony. Furthermore, altered fecal bacterial taxa and predicted metabolic pathways from VPAC1 KO mice presented significant similarities to those observed in VIP KO animals previously reported by our group.[17] Taken together, these data suggest that the VIP→VPAC1 signaling axis appears to provide a more robust and common regulatory influence on the maintenance of the gut microbiota, highlighting the

importance of this neuropeptide-receptor pathway in GIT environmental homeostasis.

The cellular influences of VIP within the GIT that may cause gut microbiota (GM) dysbiosis is likely dependent on the expression profile of its receptors, VPAC1 and VPAC2. In mice, Jayawardena et al.[5] reported exclusive VPAC1 expression in jejunum and ileum, with a 300-fold higher mRNA expression level for VPAC1 than for VPAC2 or its low-affinity receptor, pituitary adenylyl cyclase-activating polypeptide 1, in the colon. VPAC1 protein colocalized to the apical side of epithelial cells with villin, but not with the basolateral marker Na^+/K^+-ATPase.[5] In humans, VPAC1 was also the predominant VIP receptor presented on the apical side of columnar epithelial cells within the sigmoid colon, with less but equivalent expression of all 3 VIP receptors in the small intestines.[5] The present study supports VPAC1 as the predominant intestinal VIP receptor as its genetic deletion manifested in substantial gut dysbiosis. We propose that host-mediated processes, such as VIP→VPAC1 signaling, contribute to gut microbiota homeostasis by signaling through intestinal epithelial and immune cells, both of which contribute to the overall balance between tolerance vs inflammation within the GIT[23] (Figure 5).

In VIP KO mice, Goblet cell numbers were increased in the duodenum and jejunum but failed to secrete mucus protein.[12,14] Ileum and colon Goblet cell numbers were lower with reduced MUC2 expression, a major protein of mucus. Moreover, Goblet cells in ileum and colon crypts were more sensitive to VIP signaling, indicating that proliferation or differentiation and migration of goblet cells are spatially regulated with VIP being more effective within crypts.[14,24] These Goblet cell effects might also explain morphological defects observed in VIP-deficient mice throughout the GIT.[12,14] Exogenously added VIP to VIP KO mice partially rescued the aforementioned phenotypes within the colon, but not in the duodenum or jejunum, implying that developmental abnormalities and/or other gut factors were unlikely to explain the colon morphological changes.[14] VIP deficiency also resulted in reduced expression of *caudal*-related homeobox transcription factor 2 (CDX2), an intestine-specific protein that is critical for epithelial differentiation, which is in accordance with Goblet cell dysfunction from VIP KO studies and the organotypic intestinal slice model studies.[14,25] CDX2 transcriptionally activates MUC2, a migration gene called Tff3, and tight junction genes that contribute to intestinal barrier function, including claudin-3, occludin, and ZO-1.[26,27] VIPergic nerve fibers innervate all layers of the intestinal tissue that colocalize with β-III-tubulin or peripherin neuronal markers[24,28] and account for nearly 50% of enteric neurons.[12] Goblet cells in the ileum crypts were found in close proximity to neurons,[14,24] providing anatomical confirmation of neuronally derived VIP ligand in proximity to the epithelium. Murine conjunctival Goblet cells in the eye express functional VIP receptors, but it is unclear whether intestinal Goblet cells do as well.[29] Nonetheless, defective VIP→VPAC1 signaling in intestinal Goblet cells seems a likely contributor to the observed GM dysbiosis in VPAC1 KO mice (present study) and VIP KO mice.[17] That VIP- and VPAC1-deficient mice share significant similarities in their altered GM and predicted molecular pathways suggest that intestinal Goblet cells predominately express functional VPAC1 receptors. Collectively, this body of work strongly suggests that VIP signaling, presumably through the VPAC1 receptor, regulates Goblet cell biology at multiple levels. To our knowledge, the aforementioned studies have not been performed with VPAC1-deficient animals. Future research using VPAC1 KO mice, fate mapping, and single intestinal Goblet cell analyses will be instrumental in better understanding the VPAC1 receptor expression profile and its function in intestinal epithelial cells.

Reduced mucus in the gut lumen can lead to erosion of the epithelial surface, resulting in inflammation and microbiota dysbiosis as seen in MUC2-deficient mice.[30] Indeed, VIP, VPAC1, and MUC2 knockout mice exhibited altered gut microbiota compositional changes, including depletion of the anti-inflammatory, butyrate-producing *Ruminococcaceae* family,[17,30] with blooms of Gram-negative bacteria of the *Bacteroidetes* and *Proteobacteria* phyla. Breakdown of the intestinal epithelial barrier and subsequent gut microbiota dysbiosis are linked to serious health consequences, including inflammatory bowel disease,[31] type II diabetes,[32] obesity,[33] celiac disease,[17] and Graves' disease (GD).[34] An important impact from this study emphasizes the potential for targeting the VIP→VPAC1 signaling axis as a therapeutic approach as others have previously proposed.[35]

With respect to the immune system, VIP→VPAC1 signaling is important in maintaining tolerance. More than 30 years ago, Ottaway demonstrated that lowering VPAC1 receptor presentation on the plasma membrane of naive T cells significantly lowered their numbers in the intestines without altering their numbers in other compartments, implicating VPAC1 signaling as an intestinal chemoattractant receptor.[36] Once in the intestine, VIP→VPAC1 signaling induces naive CD4 T cells to express FoxP3-generating inducible T_{regs}, thereby lowering the Th17/Treg ratio and favoring tolerance.[37] This signaling is likely transmitted by VPAC1 as its expression dwarfs VPAC2 in naive CD4 T cells.[38] Treg generation can also take place via dendritic cells that have lowered costimulatory receptors through a VIP→VPAC1-mediated pathway.[39] It has been shown that differences in commensal peptide antigen presentation to T cells within the "mucosal firewall" can have profound influences on gut microbiota composition.[40,41] Noninflammatory Th17 cells induced by VIP→VPAC1 in the absence of IL-6, but in the presence of TGF-β, may also contribute to a lower Th17/Treg ratio.[42,43] Isotype switching is affected by VIP signaling on B cells that can increase IgA immunoglobulins at mucosa interphases, thereby influencing the GM.[44,45] Mast cells expressing high levels of VPAC1 have been reported to be essential for epithelial transcellular diffusion of antigens and live bacteria. When blocked by a VPAC1 receptor antagonist or a mast cell inhibitor, this bacterial movement through the cytoplasm of M

cells was blocked.[46,47] In IBS, CD, and ulcerative colitis patients, there were elevated numbers of VPAC1$^+$ mast cells in adjacent epithelium to M cells in proximity to VIP ligand. This process naturally delivers antigens to Peyer's Patches, in what appears to be a normal sampling of luminal content in healthy subjects. Enhanced transcellular diffusion by VPAC1$^+$ mast cells during an inflammatory disorder may "flood" the Peyer's Patches with antigens, causing a proinflammatory shift in the intestines affecting the GM composition. The present study is in accordance with a proinflammatory GM as both VPAC1-deficient mice (current report) and VIP-deficient mice[17] showed blooms at the ASV level that favors lipopolysaccharide (LPS)-positive, Gram-negative bacteria (eg, *Bacteroides*, *Parabacteroides*, *Parasutterella*, and *Escherichia*) that would be consistent with inflammation, and LPS biosynthesis was predicted to be more active in VIP[17] and VPAC1 KO mice. VIP signaling through VPAC1 has historically been viewed to drive most of the anti-inflammatory effects observed by VIP.[48] Supporting this idea, VIP→VPAC1 signaling in human colonic HT29-Cl.16E cells that exclusively express VPAC1 induces IL-8 synthesis and its basolateral secretion exclusively as assessed by an *in vitro* monolayer culture model.[49] IL-8 not only can act as a proinflammatory and neutrophil chemoattractant but also increases epithelial cell migration and cell growth. These authors concluded that VIP→VPAC1 may provide restorative, wound-healing-like signals to maintain epithelial barrier integrity through bolstering basolateral IL-8 expression and release[50] but acts in a suppressive, anti-inflammatory manner in the presence of proinflammatory mediators such as LPS and tumor necrosis factor alpha. We propose that defective VIP→VPAC1 signaling would jeopardize the intestinal inflammatory/tolerance balance leading to GM dysbiosis.

Peripheral blood mononuclear cells (PBMCs) from GD patients with hyperthyroidism consisting of elevated free thyroxine serum levels have defective VPAC1 signaling compared with healthy donors.[51] Serum VIP levels negatively correlated with free thyroxine serum levels, and PBMCs also expressed high levels of the intestinal chemoattractant CCR9, leading the authors to suggest that defective VPAC1 signaling in PBMCs originated within the intestines. Patients with GD also experienced gut microbiota dysbiosis with reduced levels of *Firmicutes* and elevated levels of *Bacteroidetes* that has been recently suggested to contribute to this systemic, multiorgan, autoimmune disease.[52] In addition, VIP[17] and VPAC1 deficiency (present study) shows congruent bacterial compositional changes as seen in GD patients. Pharmacological druggable targets downstream from the VPAC1 receptor might restore VPAC1 signaling within PBMCs to attenuate the symptoms of GD paving the way as a therapeutic intervention. Whether VPAC1 signaling within intestinal epithelial cells (eg, Goblet cells) is also associated with GD awaits investigation.

The more extensive gut microbiota changes in VPAC1 KO mice compared with those in VPAC2 KO mice make us conclude that circadian rhythm defects reported in VPAC2-deficient mice are not significantly driving the observed microbiota dysbiosis at least when analyzing fecal samples. This was also supported by very subtle changes in fecal bacterial composition using VPAC2 conditional KO mice in CCR6$^+$ ILC2 cells.[28] In contrast, this same study showed extensive bacterial compositional changes from cecum contents. Analyzing intestinal digesta by 16S rRNA sequencing throughout the intestines using VIP, VPAC1, and VPAC2 KO mice will greatly improve our understanding of how dysregulation of VIP signaling through either receptor influences the intestinal biogeography of the GM ecology.

VPAC1 null mice exhibited greater deaths than WT littermates. Premature deaths were attributed to intestinal obstruction. Morphological changes included thickening of the muscular plexus, epithelial cell proliferation, and mucus retention, consistent with VIP KO mice.[12] Developing mice began expressing VPAC1 in intestinal epithelium at 12.5 days and at 14.5 days in pancreatic endocrine cells, which possessed abnormal islets. Glucose blood levels were lower at baseline than controls (hypoglycemia), and giving glucose or insulin resulted in hypoglycemia and poor glucose regulation. The link between glucose metabolism, metabolic syndrome, and gut dysbiosis has been made.[53–56] Future VPAC1 cell-specific conditional knockout (eg, Goblet cell) investigations are needed to more cleanly flush out the complex cellular signaling of this receptor, thus limiting the rather extensive developmental abnormalities of VPAC1 KO mice.

We have provided 16S rRNA sequencing data from both VPAC1 and VPAC2 KO fecal samples demonstrating statistically significant gut bacterial dysbiosis. VPAC1 signaling, presumably in IECs and immune cells, resulted in (1) more severe alterations in fecal microbiota structure, (2) reduction in diversity, and (3) a greater similarity in ASV changes and predicted molecular pathways to VIP KO mice as previously published,[17] compared with VPAC2-deficient mice. In total, this report implicates the VIP→VPAC1 signaling pathway as a major driving force behind gut microbiota diversity and stability and that, when defective, may contribute to human disorders such as IBD, metabolic syndromes, and GD. Future research using VIP receptor conditional knockouts, fate mapping, and single-cell analyses are needed to begin to decipher the intricate molecular pathways of the VIP signaling axis to better identify druggable targets to treat and eventually mitigate GI tract disorders.

Methods

Mice

VIP HET breeders were a kind gift from Professor James Waschek[57] at the University of California, Los Angeles, while VPAC1 and VPAC2 HET breeders were kind gifts from professors Sue O'Dorisio[58] and Anthony Harmar,[59] and both mouse lines are commercially available (Jackson Laboratory, Bar Harbor, ME). Mice were bred at North Dakota State University, and research was approved by the NDSU Institutional Animal Care and Use Committee. All studies within this report were

Table. Primer Sequences Used for Genotyping Indicate Mouse Colonies With the Gene Name and References

Gene name	Primer sequence, 5′→3′	Reference
VIP	WT forward—TTTCAAGGTGTGGGGCTAGAGACATACA KO forward—GCCCGGAGATGAGGAAGAGGAGAACAG, Common reverse—TTACCTGATTCGTTTGCCAATGAGTGAC	55
VIPR1 (VPAC1)	WT forward—GGTTGCCATGGCTATCTTGA WT reverse—AGTGGTCTGTCTCCCCGTTGTT KO forward—TTCAACTGTTTTCCCCCATTCAC KO reverse—CCAGCTCATTCCTCCCACTCA	56
VIPR2 (VPAC2)	WT forward—CGAGAGAGCAGAGCTGACAA Common reverse—TAGGGGTGTTCCCAACTCCA KO forward—GCTTCCTCGTGCTTTACGGT	57

conducted in accordance of all state and federal regulations and guidelines. Mice were housed in polycarbonate cages containing Alpha-Dri paper bedding (Animal Care Systems, Centennial, CO), with access to 5001 LabDiet mouse chow (St. Louis, MO) and tap water *ad libitum* with a 12-hour light/dark cycle. Mice were ear clipped for identification and tail biopsies collected for PCR genotyping.[57–59]

Mouse Genotyping

DNA was extracted from tail biopsies using the Sigma-Aldrich extraction kit (St. Louis, MO) as previously published.[17] Briefly, PCR reactions were performed with a unique forward WT primer and a common reverse primer (WT reactions) or a unique forward mutant primer and a common reverse primer (KO reactions) (Table). PCR reactions (20 μl) containing 1x GoTaq G2 master mix (Promega, Madison, WI), primers (312.5 nM) and 2 μl of DNA template (1/20 dilution in TE) or nuclease-free water were amplified by PCR with the following parameters: 94 $^{\circ}C^{(3\ \text{minutes})}$ + [94 $^{\circ}C^{(15\ \text{seconds})}$, 62 $^{\circ}C^{(45\ \text{seconds})}$, 72 $^{\circ}C^{(45\ \text{seconds})}$] × 40 cycles. Reactions were separated by agarose gel electrophoresis, visualized by UV light (254 nm) using EZ-Vision dye (Amresco, Radnor, PA), and photographed with a digital camera (Alpha Innotech).

DNA Extraction

Fecal DNA was extracted using QIAamp PowerFecal kits (Qiagen, Hilden, Germany) according to the manufacturer's instructions, with the exception that, rather than performing the initial homogenization of samples using the vortex adapter described in the protocol, samples were homogenized in the provided bead tubes using a TissueLyser II (Qiagen) for 3 minutes at 30/s, before proceeding according to the protocol and eluting in 100 μL of elution buffer (Qiagen). DNA yields were quantified via fluorometry (Qubit 2.0; Invitrogen, Carlsbad, CA) using quant-iT BR dsDNA reagent kits (Invitrogen).

16S rRNA Library Preparation and Sequencing

Extracted fecal DNA was processed at the University of Missouri DNA Core Facility. Bacterial 16S rRNA amplicons targeting the V4 region were constructed via amplification with previously developed universal primers (U515F/806R), flanked by Illumina standard adapter sequences.[60,61] Oligonucleotide sequences are available at proBase.[62] Dual-indexed forward and reverse primers were used in all reactions. PCR was performed in 50-μL reactions containing 100 ng of metagenomic DNA, primers (0.2 μM each), deoxyribonucleotide triphosphates (200 μM each), and Phusion high-fidelity DNA polymerase (1U; Thermo Fisher). Amplification parameters were 98 $^{\circ}C^{(3\ \text{minutes})}$ + [98 $^{\circ}C^{(15\ \text{seconds})}$ + 50 $^{\circ}C^{(30\ \text{seconds})}$ + 72 $^{\circ}C^{(30\ \text{seconds})}$] × 25 cycles + 72 $^{\circ}C^{(7\ \text{minutes})}$. Amplicon pools (5 μL/reaction) were combined, thoroughly mixed, and then purified by addition of Axygen Axyprep MagPCR cleanup beads to an equal volume of 50 μL of amplicons and incubated for 15 minutes at room temperature. Products were then washed multiple times with 80% ethanol, and the dried pellet was resuspended in 32.5 μL of EB buffer (Qiagen), incubated for 2 minutes at room temperature, and then placed on the magnetic stand for 5 minutes. The final amplicon pool was evaluated using the Advanced Analytical Fragment Analyzer automated electrophoresis system, quantified using quant-iT HS dsDNA reagent kits, and diluted according to Illumina's standard protocol for sequencing on the MiSeq instrument.

Informatics Analysis

Primers were designed to match the 5′ ends of the forward and reverse reads. Cutadapt[63] (version 2.6; https://github.com/marcelm/cutadapt) was used to remove the primer from the 5′ end of the forward read. If found, the reverse complement of the primer to the reverse read was then removed from the forward read as were all bases downstream. Thus, a forward read could be trimmed at both ends if the insert was shorter than the amplicon length. The same approach was used on the reverse read, but with the primers in the opposite roles. Read pairs were rejected if one read or the other did not match a 5′ primer, and an error-rate of 0.1 was allowed. Two passes were made over each read to ensure removal of the second primer. A minimal overlap of 3 bp with the 3′ end of the primer sequence was required for removal. A similar strategy was used for the adapters removing any adapter sequences found on both the forward and reverse reads including those found within the reads. The trimmed and preprocessed reads were subjected to quality control assessment, per sample and collectively, using FastQC (https://github.com/s-andrews/FastQC) and MultiQC,[64] respectively. DADA2[65] (version 1.10.0) was thereafter used to denoise, dereplicate, and count

ASVs, incorporating the following parameters: (1) Forward and reverse reads were truncated to 150 bases, (2) forward and reverse reads with number of expected errors higher than 2.0 were discarded, (3) chimeras were detected using the "consensus" method and removed, and (4) with a forward and reverse reads with an overlap of at least 31 base pairs. Taxonomies were assigned to final sequences using the Silva.v132[66] database, using a pretrained data set of taxa available at https://zenodo.org/record/1172783/files/silva_nr_v132_train_set.fa.gz. Thereafter, Phyloseq[67] was used to perform richness and diversity analyses to understand the microbiota profiles using R (v4.0.1). All the aforementioned steps were implemented using a reproducible snakemake[68] workflow and can be found at https://github.com/susheelbhanu/16S_DADA2.

PICRUSt2[21] and FAPROTAX (v1.2.4)[22] were used to predict functional capacity using ASV sequences and an ASV table or the ASV table and taxonomy, respectively, with default settings as suggested by developers.

Statistics

Statistical comparisons were performed within each colony (i.e., VPAC1 and VPAC2) separately. Comparison of univariate metrics (eg, richness, α-diversity) commenced with testing for normality and equal variance using the Shapiro-Wilk and Brown-Forsyth methods, respectively. For normally distributed data, one- or two-factor ANOVA was performed to test for differences between genotypes, or interactions between genotype and sex. Kruskal-Wallis ANOVA on ranks was used for non-normally distributed data. These tests were performed using SigmaPlot 14.0 (Systat software, Inc, San Jose). For serial testing of genotype-dependent differences in the RA of operational taxonomic units within each colony, and determination of unadjusted (raw) P values, MetaboAnalyst software[69] (University of Alberta) was used. One- or two-way PERMANOVA was used to test for differences between mouse lines (eg, VIP colony vs VPAC1 colony) and main effects and interactions of genotype and sex in β-diversity within each colony. Both PCoA and PERMANOVA were performed using weighted (Bray-Curtis) similarities. All multivariate analyses were performed using quarter-root-transformed ASV counts in Past software (PAST 4.03 Free Download 2021 Latest [bytesin.com]).[70]

Code Availability

The respective scripts for FastQ file preprocessing, quality assessment, and ASV table generation via DADA2 can be found at https://github.com/susheelbhanu/16S_DADA2.

Supplementary Materials

Material associated with this article can be found in the online version at https://doi.org/10.1016/j.gastha.2021.11.005.

References

1. Martin B, Shin YK, White CM, et al. Vasoactive intestinal peptide-null mice demonstrate enhanced sweet taste preference, dysglycemia, and reduced taste bud leptin receptor expression. Diabetes 2010;59:1143–1152.
2. De Vadder F, Plessier F, Gautier-Stein A, et al. Vasoactive intestinal peptide is a local mediator in a gut-brain neural axis activating intestinal gluconeogenesis. Neurogastroenterol Motil 2015;27:443–448.
3. Vomhof-DeKrey EE, Haring JS, Dorsam GP. Vasoactive intestinal peptide receptor 1 is downregulated during expansion of antigen-specific CD8 T cells following primary and secondary Listeria monocytogenes infections. J Neuroimmunol 2011;234:40–48.
4. Dorsam GP, Benton K, Failing J, et al. Vasoactive intestinal peptide signaling axis in human leukemia. World J Biol Chem 2011;2:146–160.
5. Jayawardena D, Guzman G, Gill RK, et al. Expression and localization of VPAC1, the major receptor of vasoactive intestinal peptide along the length of the intestine. Am J Physiol Gastrointest Liver Physiol 2017; 313:G16–G25.
6. Said SI, Mutt V. Polypeptide with broad biological activity: isolation from small intestine. Science 1970; 169:1217–1218.
7. Nyberg B, Angelin B, Einarsson K. Somatostatin does not block the effect of vasoactive intestinal peptide on bile secretion in man. Eur J Clin Invest 1992;22:60–66.
8. Barbezat GO. The effect of luminal and hormonal factors on small intestinal water and electrolyte transport. Schweiz Med Wochenschr 1986;116:946–949.
9. Barbezat GO, Grossman MI. Intestinal secretion: stimulation by peptides. Science 1971;174:422–424.
10. Benarroch EE. Enteric nervous system: functional organization and neurologic implications. Neurology 2007; 69:1953–1957.
11. Van Geldre LA, Lefebvre RA. Interaction of NO and VIP in gastrointestinal smooth muscle relaxation. Curr Pharm Des 2004;10:2483–2497.
12. Lelievre V, Favrais G, Abad C, et al. Gastrointestinal dysfunction in mice with a targeted mutation in the gene encoding vasoactive intestinal polypeptide: a model for the study of intestinal ileus and Hirschsprung's disease. Peptides 2007;28:1688–1699.
13. Nussbaum JC, Van Dyken SJ, von Moltke J, et al. Type 2 innate lymphoid cells control eosinophil homeostasis. Nature 2013;502:245–248.
14. Wu X, Conlin VS, Morampudi V, et al. Vasoactive intestinal polypeptide promotes intestinal barrier homeostasis and protection against colitis in mice. PLoS One 2015; 10:e0125225.
15. Turnbaugh PJ, Ridaura VK, Faith JJ, et al. The effect of diet on the human gut microbiome: a metagenomic analysis in humanized gnotobiotic mice. Sci Transl Med 2009;1:6ra14.
16. Hooper LV, Gordon JI. Commensal host-bacterial relationships in the gut. Science 2001;292:1115–1118.
17. Bains M, Laney C, Wolfe AE, et al. Vasoactive intestinal peptide deficiency is associated with altered gut microbiota communities in male and female C57BL/6 mice. Front Microbiol 2019;10:2689.
18. Nau R, Ballmann M, Conlon JM. Binding of vasoactive intestinal polypeptide to dispersed enterocytes results in rapid removal of the NH2-terminal histidyl residue. Mol Cell Endocrinol 1987;52:97–103.
19. Harmar AJ, Sheward WJ, Morrison CF, et al. Distribution of the VPAC2 receptor in peripheral tissues of the mouse. Endocrinology 2004;145:1203–1210.

20. Bolyen E, Rideout JR, Dillon MR, et al. Reproducible, interactive, scalable and extensible microbiome data science using QIIME 2. Nat Biotechnol 2019;37:852–857.
21. Douglas GM, Maffei VJ, Zaneveld JR, et al. PICRUSt2 for prediction of metagenome functions. Nat Biotechnol 2020;38:685–688.
22. Louca S, Parfrey LW, Doebeli M. Decoupling function and taxonomy in the global ocean microbiome. Science 2016;353:1272–1277.
23. Su X, Yin X, Liu Y, et al. Gut dysbiosis contributes to the imbalance of Treg and Th17 cells in Graves' disease patients by propionic acid. J Clin Endocrinol Metab 2020;105:dgaa511.
24. Schwerdtfeger LA, Tobet SA. Vasoactive intestinal peptide regulates ileal goblet cell production in mice. Physiol Rep 2020;8:e14363.
25. Grainger S, Savory JG, Lohnes D. Cdx2 regulates patterning of the intestinal epithelium. Dev Biol 2010; 339:155–165.
26. Shimada T, Koike T, Yamagata M, et al. Regulation of TFF3 expression by homeodomain protein CDX2. Regul Pept 2007;140:81–87.
27. Mesquita P, Jonckheere N, Almeida R, et al. Human MUC2 mucin gene is transcriptionally regulated by Cdx homeodomain proteins in gastrointestinal carcinoma cell lines. J Biol Chem 2003;278:51549–51556.
28. Talbot J, Hahn P, Kroehling L, et al. Feeding-dependent VIP neuron-ILC3 circuit regulates the intestinal barrier. Nature 2020;579:575–580.
29. Li D, Jiao J, Shatos MA, et al. Effect of VIP on intracellular [Ca2+], extracellular regulated kinase 1/2, and secretion in cultured rat conjunctival goblet cells. Invest Ophthalmol Vis Sci 2013;54:2872–2884.
30. Wu M, Wu Y, Li J, et al. The dynamic changes of gut microbiota in Muc2 deficient mice. Int J Mol Sci 2018;19.
31. Parikh K, Antanaviciute A, Fawkner-Corbett D, et al. Colonic epithelial cell diversity in health and inflammatory bowel disease. Nature 2019;567:49–55.
32. Sharma S, Tripathi P. Gut microbiome and type 2 diabetes: where we are and where to go? J Nutr Biochem 2019;63:101–108.
33. Chelakkot C, Ghim J, Ryu SH. Mechanisms regulating intestinal barrier integrity and its pathological implications. Exp Mol Med 2018;50:103.
34. Chang SC, Lin SF, Chen ST, et al. Alterations of gut microbiota in patients with Graves' disease. Front Cell Infect Microbiol 2021;11:663131.
35. Iwasaki M, Akiba Y, Kaunitz JD. Recent advances in vasoactive intestinal peptide physiology and pathophysiology: focus on the gastrointestinal system. F1000Res 2019;8:F1000 Faculty Rev-1629.
36. Ottaway CA. In vitro alteration of receptors for vasoactive intestinal peptide changes the in vivo localization of mouse T cells. J Exp Med 1984;160:1054–1069.
37. Chorny A, Gonzalez-Rey E, Ganea D, et al. Vasoactive intestinal peptide generates CD4+CD25+ regulatory T cells in vivo: therapeutic applications in autoimmunity and transplantation. Ann N Y Acad Sci 2006; 1070:190–195.
38. Dorsam ST, Vomhof-Dekrey E, Hermann RJ, et al. Identification of the early VIP-regulated transcriptome and its associated, interactome in resting and activated murine CD4 T cells. Mol Immunol 2010;47:1181–1194.
39. Delgado M, Gonzalez-Rey E, Ganea D. The neuropeptide vasoactive intestinal peptide generates tolerogenic dendritic cells. J Immunol 2005;175:7311–7324.
40. Belkaid Y, Hand TW. Role of the microbiota in immunity and inflammation. Cell 2014;157:121–141.
41. Khan AA, Yurkovetskiy L, O'Grady K, et al. Polymorphic immune mechanisms regulate commensal repertoire. Cell Rep 2019;29:541–550.e4.
42. Leceta J, Gomariz RP, Martinez C, et al. Vasoactive intestinal peptide regulates Th17 function in autoimmune inflammation. Neuroimmunomodulation 2007;14:134–138.
43. Yadav M, Rosenbaum J, Goetzl EJ. Cutting edge: vasoactive intestinal peptide (VIP) induces differentiation of Th17 cells with a distinctive cytokine profile. J Immunol 2008;180:2772–2776.
44. Kimata H, Fujimoto M. Vasoactive intestinal peptide specifically induces human IgA1 and IgA2 production. Eur J Immunol 1994;24:2262–2265.
45. Fujieda S, Waschek JA, Zhang K, et al. Vasoactive intestinal peptide induces S(alpha)/S(mu) switch circular DNA in human B cells. J Clin Invest 1996;98:1527–1532.
46. Bednarska O, Walter SA, Casado-Bedmar M, et al. Vasoactive intestinal polypeptide and mast cells regulate increased passage of colonic bacteria in patients with irritable bowel syndrome. Gastroenterology 2017; 153:948–960.e3.
47. Casado-Bedmar M, Heil SDS, Myrelid P, et al. Upregulation of intestinal mucosal mast cells expressing VPAC1 in close proximity to vasoactive intestinal polypeptide in inflammatory bowel disease and murine colitis. Neurogastroenterol Motil 2019;31:e13503.
48. Delgado M, Pozo D, Ganea D. The significance of vasoactive intestinal peptide in immunomodulation. Pharmacol Rev 2004;56:249–290.
49. Toumi F, Neunlist M, Denis MG, et al. Vasoactive intestinal peptide induces IL-8 production in human colonic epithelial cells via MAP kinase-dependent and PKA-independent pathways. Biochem Biophys Res Commun 2004;317:187–191.
50. Mullol J, Baraniuk JN, Pitale M, et al. Vasoactive intestinal peptide (VIP) induces IL-6 and IL-8, but not G-CSF and GM-CSF release from a human bronchial epithelial cell line. Neuropeptides 1997;31:119–124.
51. Carrión M, Ramos-Leví AM, Seoane IV, et al. Vasoactive intestinal peptide axis is dysfunctional in patients with Graves' disease. Sci Rep 2020;10:13018.
52. Jiang W, Yu X, Kosik RO, et al. Gut microbiota may play a significant role in the pathogenesis of Graves' disease. Thyroid 2021;31:810–820.
53. Ramakrishna BS. Role of the gut microbiota in human nutrition and metabolism. J Gastroenterol Hepatol 2013; 28 Suppl 4:9–17.
54. Nishitsuji K, Xiao J, Nagatomo R, et al. Analysis of the gut microbiome and plasma short-chain fatty acid profiles in a spontaneous mouse model of metabolic syndrome. Sci Rep 2017;7:15876.
55. Li G, Xie C, Lu S, et al. Intermittent fasting promotes white adipose browning and decreases obesity by shaping the gut microbiota. Cell Metab 2017;26:672–685.e4.

56. Lee JC, Lee HY, Kim TK, et al. Obesogenic diet-induced gut barrier dysfunction and pathobiont expansion aggravate experimental colitis. PLoS One 2017; 12:e0187515.
57. Colwell CS, Michel S, Itri J, et al. Disrupted circadian rhythms in VIP- and PHI-deficient mice. Am J Physiol Regul Integr Comp Physiol 2003;285:R939–R949.
58. Fabricius D, Karacay B, Shutt D, et al. Characterization of intestinal and pancreatic dysfunction in VPAC1-null mutant mouse. Pancreas 2011;40:861–871.
59. Harmar AJ, Marston HM, Shen S, et al. The VPAC(2) receptor is essential for circadian function in the mouse suprachiasmatic nuclei. Cell 2002;109:497–508.
60. Walters WA, Caporaso JG, Lauber CL, et al. PrimerProspector: de novo design and taxonomic analysis of barcoded polymerase chain reaction primers. Bioinformatics 2011;27:1159–1161.
61. Caporaso JG, Lauber CL, Walters WA, et al. Global patterns of 16S rRNA diversity at a depth of millions of sequences per sample. Proc Natl Acad Sci U S A 2011; 108 Suppl 1:4516–4522.
62. Loy A, Maixner F, Wagner M, et al. probeBase–an online resource for rRNA-targeted oligonucleotide probes: new features 2007. Nucleic Acids Res 2007;35:D800–D804.
63. Martin M. Cutadapt removes adapter sequences from high-throughput sequencing reads. EMBnet J 2011;17:10–12.
64. Ewels P, Magnusson M, Lundin S, et al. MultiQC: summarize analysis results for multiple tools and samples in a single report. Bioinformatics 2016;32:3047–3048.
65. Callahan BJ, McMurdie PJ, Rosen MJ, et al. DADA2: high-resolution sample inference from Illumina amplicon data. Nat Methods 2016;13:581–583.
66. Pruesse E, Quast C, Knittel K, et al. SILVA: a comprehensive online resource for quality checked and aligned ribosomal RNA sequence data compatible with ARB. Nucleic Acids Res 2007;35:7188–7196.
67. McMurdie PJ, Holmes S. phyloseq: an R package for reproducible interactive analysis and graphics of microbiome census data. PLoS One 2013;8:e61217.
68. Koster J, Rahmann S. Snakemake–a scalable bioinformatics workflow engine. Bioinformatics 2012; 28:2520–2522.
69. Xia J, Psychogios N, Young N, et al. MetaboAnalyst: a web server for metabolomic data analysis and interpretation. Nucleic Acids Res 2009;37:W652–W660.
70. Hammer O, Harper DAT. PAST: paleontological statistics software package for education and data analysis. Palaeontol Electron 2011;4:1–9.

Received August 20, 2021. Accepted November 11, 2021.

Correspondence:
Address correspondence to: Glenn P. Dorsam, PhD, Department of Microbiological Sciences, 1230 Albrecht Blvd, North Dakota State University, Fargo, North Dakota 58102. e-mail: glenn.dorsam@ndsu.edu.

Authors' Contributions:
Manpreet Bains managed the daily operations of the mouse vivarium that included daily documentation, topping off food and water, weekly cage changes, weaning, tail biopsy collection, DNA extraction, and PCR genotyping and fecal collections. Manpreet Bains assisted with the writing of the manuscript as part of his doctoral dissertation. James A. Waschek provided expert experimental design review and interpretation of results. Justin Daniels performed confirmatory genotyping of all samples used in the study. Aaron C. Ericsson oversaw DNA extraction, 16S rRNA library preparation and sequencing, bioinformatics, and statistics; analyzed and interpreted data; and co-wrote the manuscript. Susheel B Busi and Zachary McAdams performed bioinformatics and helped with analysis and writing the manuscript. Glenn P. Dorsam conceived and designed the study, helped interpret data, and co-wrote the manuscript. All authors edited the final manuscript version.

Conflicts of Interest:
The authors disclose no conflicts.

Funding:
Manpreet Bains received funding for graduate student training from the Department of Microbiological Sciences. Glenn P. Dorsam received a seed grant from the Vice President of Research at North Dakota State University. James A. Waschek received funding from the National Multiple Sclerosis Society (RG-1901-33326).

Ethical Statement:
The corresponding author, on behalf of all authors, jointly and severally, certifies that their institution has approved the protocol for any investigation involving humans or animals and that all experimentation was conducted in conformity with ethical and humane principles of research.

Data Transparency Statement:
All data supporting the present manuscript have been deposited in the National Center for Biotechnology Information (NCBI) Sequence Read Archive under BioProject ID PRJNA679452 (VPAC1 and VPAC2 lines) or BioProject ID PRJNA575206 (VIP line) and can be accessed at the following URLs http://www.ncbi.nlm.nih.gov/bioproject/679452 or http://www.ncbi.nlm.nih.gov/bioproject/575206, respectively.